Journal Pre-proofs

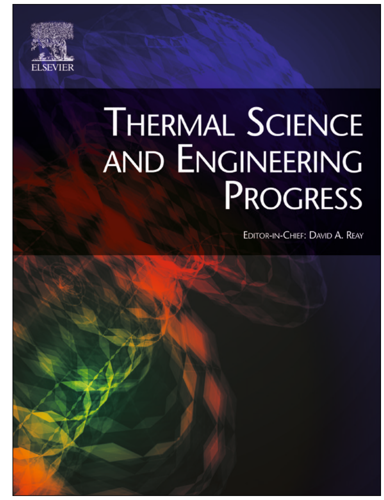

Statistical Analysis of MHD Convective Ferro-nanofluid Flow through an Inclined Channel with Hall Current, Heat Source and Soret Effect

A.S. Sabu, Alphonsa Mathew, T.S. Neethu, K. Anil George

PII:	S2451-9049(20)30336-X
DOI:	https://doi.org/10.1016/j.tsep.2020.100816
Reference:	TSEP 100816
To appear in:	*Thermal Science and Engineering Progress*
Received Date:	10 July 2020
Revised Date:	4 September 2020
Accepted Date:	13 December 2020

Please cite this article as: A.S. Sabu, A. Mathew, T.S. Neethu, K. Anil George, Statistical Analysis of MHD Convective Ferro-nanofluid Flow through an Inclined Channel with Hall Current, Heat Source and Soret Effect, *Thermal Science and Engineering Progress* (2020), doi: https://doi.org/10.1016/j.tsep.2020.100816

Statistical Analysis of MHD Convective Ferro-nanofluid Flow through an Inclined Channel with Hall Current, Heat Source and Soret Effect

A S Sabu[1], Alphonsa Mathew*[1], Neethu T S[1], Anil George K[2]

*[1]Corresponding Author, [1]Department of Mathematics, St. Thomas College, Thrissur, Kerala, India 680001. Email: alphonsa@stthomas.ac.in

[2]Department of Computer Science, St Thomas College, Thrissur, Kerala, India-680 001

Emails: sabuas@stthomas.ac.in, neethuts13@gmail.com, anilgeorgek@stthomas.ac.in

Abstract: The role of hall current, heat source and Soret effects on MHD convective ferro-nanofluid (Fe3O4-water) flow through an inclined channel with porous medium has been theoretically and statistically examined. Velocity, thermal and concentration boundary layer in nanofluids are considered to be oscillatory. Heat due to radiation is induced by the huge disparity in temperature between the plates. Hall current is generated by the uniform application of a strong magnetic field perpendicular to the flow of fluid. Boundary layer equations are changed to non-dimensional type and it is resolved by perturbation approximation. The outcomes are displayed in the form of tables and figures using MATLAB software. The outcome of pertinent parameters on concentration, temperature and velocity profiles are evaluated through graphs. Besides, wall heat, mass transfer rates and surface drag are investigated through statistical tools like regression and probable error. Results explain that heat source and hall current have a negative impact on skin friction whereas heat source has a positive impact on Nusselt number. Also, Soret number has a negative impact on Sherwood number.

Keywords: Hall current effect, Heat source; Magnetohydrodynamic (MHD) flow, Nanofluid, Regression Analysis, Probable Error

Nomenclature

u^*, v^*, w^*	velocity components (m/s)	Cf	Skin friction coefficient
T	fluid temperature (K)	K_r	chemical reaction parameter
C'	fluid concentration $(Moles/kg)$	K	Thermal conductivity $(Wm^{-1} K^{-1})$
g	acceleration due to gravity $(m\, s^{-2})$	Nu	Nusselt number
t	time(s)	B_0	strength of magnetic field
H	hall current parameter	S_c	Schmidt number
T_0	temperature of the fluid near the origin (K)	G_r	Grashof number
T_d	temperature of the fluid at d (K)	G_m	Modified Grashof number
C_0	nanoparticle concentration near the origin $(Moles/kg)$	K_1	dimensionless porosity parameter
C_d	Nanoparticle concentration at d $(Moles/kg)$	K_1^*	permeability of the medium
D_T	coefficient of chemical molecular diffusivity	r	Correlation Coefficient
D_B	coefficient of thermal diffusivity	PE	Probable Error
$(\rho c)_f$	heat capacity of the fluid $(Jk\, gm^{-3}K^{-1})$	**Greek symbols**	
$(\rho c)_p$	effective heat capacity of nanoparticles $(Jkgm^{-3}K^{-1})$	σ	electrical conductivity
P_r	Prandtl number	ϕ	volume fraction of nanoparticles
P	pressure (Nm^{-2})	μ	dynamic viscosity $(kgm^{-1}s^{-1})$
U	velocity of the plate	ρ	density (kgm^{-3})
M	Hartmann number	λ	injection/suction parameter
Q	volumetric rate of heat generation /absorption	β_T	coefficient of volume expansion
q_z^*	radiative heat flux	β_C	volumetric coefficient of expansion with concentration
N	radiation parameter	α	Angle of inclination
S	heat source/sink parameter	**Subscripts**	
C_p	specific heat at constant pressure	nf	nanofluid
S_o	Soret number	f	base fluid
Sh	Sherwood number	s	nanoparticle
R_e	Reynolds number	w	quantities at wall

1. Introduction

Metals and metal oxides show larger thermal conductivity in comparison with fluids. Nanofluid was first discovered by Choi [1] for its exceptional cooling performance and heat transfer ability. Nanofluid has been proposed as a liquid suspension of nanoparticles of size 1-100 nm by Choi. Base fluid and nanoparticles in nanofluid exhibit unique chemical and physical properties [2]. Concerning the heat transfer property of nanofluid, Eastman [3] observed that when 5% of Copper Oxide nanoparticles was used in water, the heat transfer property increased by 60 %. Nanofluids are used in solar thermal collectors, heat pipes, automotive radiators and tube heat exchangers [4]. MHD nanofluid flow is used in magnetic drug targeting, MHD pumps, MHD sensors, plasma, crystal growth and mixing of physiological samples [5,6]. Nanoparticles can bind proteins, drug and spot cancer cells [7]. MHD fluid flow can be found in [8–10].

Das [11] reviewed the transient free convection nanofluid flow through a vertical channel in the presence of thermal radiation. Convection flow through the vertical channel is decisive in the cooling systems of heat exchangers and solar cells. Warm blood circulation in mammals and engine cooling are examples of convection. Forced and free convections play a decisive role in the convection flows. Enforced convection with heat transfer properties in a porous channel is evaluated by Maghrebi [12] and free convection flow is found in [13–15]. Convective flow with different nanofluids are used in [16]. Eshetu Haile and Shankar [17] examined the MHD nanofluid flow with heat and mass transfer through a porous medium with thermal radiation, viscous dissipation and chemical reaction effects. The study showed that the effect of heat and mass transfer with chemical reaction has a significant role in processes like transfer of energy in wet cooling tower, drying, the flow in desert cooler and electric power generation. It has a major role in industrial process like fabrication of ceramics or glassware and the production of polymers [17]. Nanofluid flow with chemical reaction can be found in

[18–21] and radiation effects are studied in [22–26]. MHD flow past cosinusoidally fluctuating heated plate with radiation was researched by Ram et al. [27]. An oscillatory MHD flow through a rotating channel in the presence of Hall current has been analyzed previously by Pal and Talukdar [28]. Electrically conducting fluid flow through a rotating porous channel has wide industrial uses like nuclear reactors, geothermal systems and filtration etc.[29]. Soret and heat source effects on MHD flow are studied in [30,31].

MHD convective flow through an inclined channel can be found in [32–35]. In this paper, chemical reaction/radiation impacts on MHD convective nanofluid flow in and through an inclined channel with Hall current, heat source and Soret effect are analyzed using ferro-nanofluid. In addition, the resultant thermal conductivity is found using the Hamilton-Crosser model [36].

2. Mathematical Problem Statement

An unsteady free convective, incompressible and electrically conducting ferro-nanofluid flow through an inclined channel packed with porous medium is considered. The problem is studied under the following assumptions:

(i) Ferro-nanofluid flow is observed in the X^* direction.

(ii) Two infinite electrically non-conducting and permeable parallel plates at a distance d apart inclined at an angle α are considered (see Fig. 1).

(iii) One plate is held stationary while the other is oscillating in its own plane with a velocity $U^*(t^*)$.

(iv) Ferro-nanofluid is injected into the stationary plate with a velocity w_0 and is sucked by the oscillating plate with a velocity w_0.

(v) A uniform magnetic field of strength B_0 is exerted in the Z^* axis (orthogonal to the flow) and Hall current is generated due to this magnetic field.

(vi) Effect of induced electric and magnetic field are ignored due to small magnetic Reynolds number.

(vii) Temperature and concentration at the stationary plate periodically varies with time t^*.

(viii) Plates are maintained at high-temperature variation to induce heat transfer via radiation. The radiative heat flux is considered in the Z^* direction.

(ix) Density variation with temperature and concentration in body force term is considered and all other fluid properties are assumed to be constant.

(x) Additional heat source (Q^*) and the order of reactive species in an irreversible chemical reaction are considered.

(xi) Viscous dissipation, Joule heating, electric and polarisation effects are ignored [37].

Using Boussinesq's approximation, the flow is described [13, 28, 38] as:

$$\rho_{nf}\left(\frac{\partial u^*}{\partial t^*} + w_0\frac{\partial u^*}{\partial z^*}\right) = -\frac{\partial p^*}{\partial x^*} + \mu_{nf}\frac{\partial^2 u^*}{\partial z^{*2}} + (\rho\beta_T)_{nf}g\left(T^* - T_d\right)sin\alpha + (\rho\beta_C)_{nf}g\left(C^* - C_d\right)\sin\alpha + \frac{\sigma B_0{}^2(Hv^* - u^*)}{1+H^2} - \frac{\mu_{nf}}{K_1{}^*}u^* \tag{1}$$

$$\rho_{nf}\left(\frac{\partial v^*}{\partial t^*} + w_0\frac{\partial v^*}{\partial z^*}\right) = -\frac{\partial p^*}{\partial y^*} + \mu_{nf}\frac{\partial^2 v^*}{\partial z^{*2}} - \frac{\sigma B_0{}^2(Hu^* + v^*)}{1+H^2} - \frac{\mu_{nf}}{K_1{}^*}v^* \tag{2}$$

$$(\rho C_p)_{nf}\left(\frac{\partial T^*}{\partial t^*} + w_0\frac{\partial T^*}{\partial z^*}\right) = K_{nf}\frac{\partial^2 T^*}{\partial z^{*2}} - \frac{\partial q^*}{\partial z^*} + Q^*\left(T^* - T_d\right) \tag{3}$$

$$\frac{\partial C^*}{\partial t^*} + w_0\frac{\partial C^*}{\partial z^*} = D_B\frac{\partial^2 C^*}{\partial z^{*2}} + D_T\frac{\partial^2 T^*}{\partial z^{*2}} - K_l\left(C^* - C_d\right) \tag{4}$$

where the terms are explained in nomenclature.

Optically thin nanofluid has been considered and hence radiative heat flux [37] is taken as $\frac{\partial q^*}{\partial z^*} = 4\alpha^2(T_0 - T_d)$.

Corresponding boundary conditions are:

$$\left.\begin{aligned} u^* = v^* = 0, T^* = T_0 + \epsilon(T_0 - T_d)cos\omega^* t^*, C^* = C_0 + \epsilon(C_0 - C_d)cos\omega^* t^*, z^* = 0 \\ u^* = U_0(1 + \epsilon cos\omega^* t^*),\ v^* = 0,\ T^* = T_d, C^* = C_d,\ z^* = d \end{aligned}\right\}$$
(5)

Following quantities are used to make equations (1) to (4) in dimensionless form:

$$\left.\begin{aligned} K_r = \frac{K_l\gamma}{{w_0}^2}, D_B = \frac{\gamma}{S_c}, N = \frac{2\alpha d}{\sqrt{K}}, R_e = \frac{U_0 d}{\gamma}, \lambda = \frac{w_0 d}{\gamma}, M = B_0 d\sqrt{\frac{\sigma}{\mu}}, \\ z = \frac{z^*}{d}, x = \frac{x^*}{d}, t = t^*\omega^*, u = \frac{u^*}{U_0}, v = \frac{v^*}{U_0}, \omega = \frac{\omega^* d^2}{\gamma}, \\ U = \frac{U^*}{U_0}, K_1 = \frac{{K_1}^*}{d^2}, S = \frac{Q^* d^2}{K}, P_r = \frac{\mu C_p}{K}, G_m = \frac{\gamma g\beta(C_0 - C_d)}{U_0 {w_0}^2} \\ S_0 = \frac{D_T(T_0 - T_d)}{(C_0 - C_d)\gamma}, \theta' = \frac{T^* - T_d}{(T_0 - T_d)}, C' = \frac{C^* - C_d}{(C_0 - C_d)}, G_r = \frac{\gamma g\beta(T_0 - T_d)}{U_0 {w_0}^2} \end{aligned}\right\} \quad (6)$$

The nanofluid constants are stated [39] as follows:

$$\rho_{nf} = (1-\phi)\rho_f + \phi\rho_s, \mu_{nf} = \frac{\mu_f}{(1-\phi)^{2.5}}, (\rho C_p)_{nf} = (1-\phi)(\rho C_p)_f + \phi(\rho C_p)_s$$

$$\lambda_n = \frac{K_{nf}}{K_f} = \frac{K_s + (h-1)K_f - (h-1)(K_f - K_s)\phi}{K_s + (h-1)K_f + (K_f - K_s)\phi}, \frac{\sigma_{nf}}{\sigma_f} = 1 + \frac{3\left(\frac{\sigma_s}{\sigma_f} - 1\right)\phi}{\frac{\sigma_s}{\sigma_f} - 2 - \left(\frac{\sigma_s}{\sigma_f} - 1\right)\phi},$$

$$(\rho\beta_T)_{nf} = (1-\phi)(\rho\beta_T)_f + \phi(\rho\beta_T)_s$$

Let $\beta_T = \beta_C$ and assume that

$$\phi_1 = 1 - \phi + \phi\frac{\rho_s}{\rho_f}, \phi_2 = \frac{1}{(1-\phi)^{2.5}}, \phi_3 = 1 - \phi + \phi\frac{(\rho\beta_T)_s}{(\rho\beta_T)_f},$$

$$\phi_4 = 1 - \phi + \phi\frac{(\rho C_p)_s}{(\rho C_p)_f}, \phi_5 = \frac{\sigma_{nf}}{\sigma_f}$$

Let $l' = u + iv$ and $h = 3$, then the equations (1) to (4) along with condition (5) are transformed into the non-dimensional form given by:

$$\begin{aligned} \phi_1\left(\omega\frac{\partial l'}{\partial t} + \lambda\frac{\partial l'}{\partial z}\right) = \phi_1\omega\frac{\partial U}{\partial t} + \phi_2\frac{\partial^2 l'}{\partial z^2} + \phi_3\lambda^2 sin\alpha(Gr\,\theta' + Gm\,C') \\ - (l' - U)\left(\frac{\phi_2}{K_1} + \frac{\phi_5 M^2}{1 + H^2}(1 + iH)\right) \end{aligned} \quad (7)$$

$$\phi_4\left(\omega\frac{\partial\theta'}{\partial t} + \lambda\frac{\partial\theta'}{\partial z}\right) = \frac{1}{P_r}\left(\lambda_n\frac{\partial^2\theta'}{\partial z^2} - N^2\theta' + S\theta'\right) \quad (8)$$

$$\omega\frac{\partial C'}{\partial t}+\lambda\frac{\partial C'}{\partial z}=\frac{1}{S_c}\frac{\partial^2 C'}{\partial z^2}+S_0\frac{\partial^2\theta'}{\partial z^2}-K_r\lambda^2C' \tag{9}$$

The corresponding boundary conditions are:

$$\left.\begin{array}{r} l'=0,\ \theta'=C'=1+\epsilon cost,\ z=0 \\ l'=1+\epsilon cost,\ \theta'=0,\ C'=0,\ z=1 \end{array}\right\} \tag{10}$$

3. The Resolution

Solutions of equation (7) to (9) are approximated [40] as:

$$\delta'=\delta'_0(z)+\frac{\epsilon}{2}\left(\delta'_1(z)e^{(it)}+\delta'_2(z)e^{(-it)}\right) \tag{11}$$

Replacing δ' by the terms l',θ' and C' and applying in equations $(7)-(10)$ we have:

$$\theta'_0=m_1e^{(\eta_1z)}+m_2e^{(\eta_2z)} \tag{12}$$

$$\theta'_1=m_3e^{(\eta_3z)}+m_4e^{(\eta_4z)} \tag{13}$$

$$\theta'_2=m_5e^{(\eta_5z)}+m_6e^{(\eta_6z)} \tag{14}$$

$$C'_0=\zeta_1e^{(q_1z)}+\zeta_2e^{(q_2z)}+A_{11}e^{(\eta_1z)}+A_{12}e^{(\eta_2z)} \tag{15}$$

$$C'_1=\zeta_3e^{(q_3z)}+\zeta_4e^{(q_4z)}+A_{21}e^{(\eta_3z)}+A_{22}e^{(\eta_4z)} \tag{16}$$

$$C'_2=\zeta_5e^{(q_5z)}+\zeta_6e^{(q_6z)}+A_{31}e^{(\eta_5z)}+A_{32}e^{(\eta_6z)} \tag{17}$$

$$\begin{aligned} l'_0=&\,h_1e^{(\chi_1z)}+h_2e^{(\chi_2z)}+D_{11}+D_{12}e^{(\eta_1z)}+D_{13}e^{(\eta_2z)} \\ &+D_{14}e^{(q_1z)}+D_{15}e^{(q_2z)}+D_{16}e^{(\eta_1z)}+D_{17}e^{(\eta_2z)} \end{aligned} \tag{18}$$

$$\begin{aligned} l'_1=&\,h_3e^{(\chi_3z)}+h_4e^{(\chi_4z)}+D_{21}+D_{22}e^{(\eta_3z)}+D_{23}e^{(\eta_4z)} \\ &+D_{24}e^{(q_3z)}+D_{25}e^{(q_4z)}+D_{26}e^{(\eta_3z)}+D_{27}e^{(\eta_4z)} \end{aligned} \tag{19}$$

$$\begin{aligned} l'_2=&\,h_5e^{(\chi_5z)}+h_6e^{(\chi_6z)}+D_{31}+D_{32}e^{(\eta_5z)}+D_{33}e^{(\eta_6z)} \\ &+D_{34}e^{(q_5z)}+D_{35}e^{(q_6z)}+D_{36}e^{(\eta_5z)}+D_{37}e^{(\eta_6z)} \end{aligned} \tag{20}$$

$$\left.\begin{array}{r}\text{Local Nusselt number } Nu = \frac{x^* q_w}{K_f(T_0 - T_d)} \\ \text{local Sherwood number } Sh = \frac{x^* q_m}{D_B(C_0 - C_d)} \\ \text{Skin} - \text{friction coefficient } Cf = \frac{\tau_w}{\rho_f U_0^2}\end{array}\right\} \tag{21}$$

where

$$q_w = - K_{nf}\frac{\partial T^*}{\partial z^*},\ q_m = - D_B\frac{\partial C^*}{\partial z^*},\ \tau_w = \mu_{nf}\frac{\partial u^*}{\partial z^*}$$

Using the non-dimensional quantities (6), the above expressions are transformed into:

$$Nu = - \lambda_n\frac{\partial \theta'}{\partial z},\ Sh = - \frac{\partial C'}{\partial z}, \quad Cf = \frac{\phi_2 \partial l'}{R_e \partial z}$$

Skin friction Coefficient C_f at $z = 1$

$$Cf = \frac{\phi_2}{R_e}\left(\frac{\partial l'}{\partial z}\right)_{z = 1}$$

$$Cf = \frac{\phi_2}{R_e}\left(Cf_0 + \frac{\varepsilon}{2}\left(Cf_1 e^{(it)} + Cf_2 e^{(-it)}\right)\right) \tag{22}$$

where,

$$Cf_0 = \chi_1 h_1 e^{(\chi_1)} + \chi_2 h_2 e^{(\chi_2)} + \eta_1 D_{12} e^{(\eta_1)} + \eta_2 D_{13} e^{(\eta_2)} + q_1 D_{14} e^{(q_1)} + q_2 D_{15} e^{(q_2)} + \eta_1 D_{16} e^{(\eta_1)} + \eta_2 D_{17} e^{(\eta_2)}$$

$$Cf_1 = \chi_3 h_3 e^{(\chi_3)} + \chi_4 h_4 e^{(\chi_4)} + \eta_3 D_{22} e^{(\eta_3)} + \eta_4 D_{23} e^{(\eta_4)} + q_3 D_{24} e^{(q_3)} + q_4 D_{25} e^{(q_4)} + \eta_3 D_{26} e^{(\eta_3)} + \eta_4 D_{27} e^{(\eta_4)}$$

$$Cf_2 = \chi_5 h_5 e^{(\chi_5)} + \chi_6 h_6 e^{(\chi_6)} + \eta_5 D_{32} e^{(\eta_5)} + \eta_6 D_{33} e^{(\eta_6)} + q_5 D_{34} e^{(q_5)} + q_6 D_{35} e^{(q_6)} + \eta_5 D_{36} e^{(\eta_5)} + \eta_6 D_{37} e^{(\eta_6)}$$

Sherwood Number Sh at $z = 1$

$$Sh = -\left(\frac{\partial C'}{\partial z}\right)_{z=1}$$

$$Sh = -\left(Sh_0 + \frac{\varepsilon}{2}\left(Sh_1 e^{(it)} + Sh_2 \mathrm{e}^{(-\mathrm{it})}\right)\right) \tag{23}$$

where

$$Sh_0 = q_1\zeta_1\mathrm{e}^{(\mathrm{q}_1)} + q_2\zeta_2\mathrm{e}^{(\mathrm{q}_2)} + \eta_1 A_{11}e^{(\eta_1)} + \eta_2 A_{12}\mathrm{e}^{(\eta_2)}$$

$$Sh_1 = q_3\zeta_3\mathrm{e}^{(\mathrm{q}_3)} + q_4\zeta_4\mathrm{e}^{(\mathrm{q}_4)} + \eta_3 A_{21}\mathrm{e}^{(\eta_3)} + \eta_4 A_{22}\mathrm{e}^{(\eta_4)}$$

$$Sh_2 = q_5\zeta_5\mathrm{e}^{(\mathrm{q}_5)} + q_6\zeta_6\mathrm{e}^{(\mathrm{q}_6)} + \eta_5 A_{31}\mathrm{e}^{(\eta_5)} + \eta_6 A_{32}\mathrm{e}^{(\eta_6)}$$

Nusselt Number Nu at z = 1

$$Nu = -\lambda_n\left(\frac{\partial \theta'}{\partial z}\right)_{z=1}$$

$$Nu = -\lambda_n\left(Nu_0 + \frac{\varepsilon}{2}\left(Nu_1 e^{(it)} + Nu_2\mathrm{e}^{(-\mathrm{it})}\right)\right) \tag{24}$$

where

$$Nu_0 = \eta_1 m_1\mathrm{e}^{(\eta_1)} + \eta_2 m_2\mathrm{e}^{(\eta_2)}$$
$$Nu_1 = \eta_3 m_3\mathrm{e}^{(\eta_3)} + \eta_4 m_4\mathrm{e}^{(\eta_4)}$$
$$Nu_2 = \eta_5 m_5\mathrm{e}^{(\eta_5)} + \eta_6 m_6\mathrm{e}^{(\eta_6)}$$

The amplitude (τ_{0r}) and phase difference (β_0) of shear stress at $z = 0$ in the case of steady flow is defined as $\tau_{0r} = \sqrt{\tau_{0x}^2 + \tau_{0y}^2}$ and $\beta_o = \tan^{-1}\left(\frac{\tau_{0y}}{\tau_{0x}}\right)$; where $\left(\frac{\partial l_0'}{\partial z}\right)_{z=0} = \tau_{0x} + i\tau_{0y}$,

$$\left(\frac{\partial l_0'}{\partial z}\right)_{z=0} = \chi_1 h_1 + \chi_2 h_2 + \eta_1 D_{12} + \eta_2 D_{13} + D_{14} q_1 + D_{15} q_2 + D_{16}\eta_1 + D_{17}\eta_2.$$

To validate the numerical values, comparison study has been carried out in Table 11 and Table 12 with previously published papers [41] and [28]. The numerical values are found to be in excellent agreement.

4. Results and Discussion

Fluid profiles for l',θ' and $C'$of ferro-nanofluid are plotted by choosing the following values:

$$t = ,P_r = 6.07,\ G_r = 5,\ G_m = 5, \lambda = 1, N = 0.5, K_r = 1, K_1 = 0.7, M = 3,\ H = 0.5, S_0 = 1, S = 3, \omega = 10, S_c = 0.22, \phi = 0.04, h = 3, \alpha = 45^0,\ R_e = 10, \epsilon = 0.01$$

Thermo physical properties [42–44] of nanoparticles and base fluid at 25^0 are shown in the Table 1. Values of Nu, Sh and $Cf$are given in tables 2-4. The effect of volume fraction and non-dimensional parameters has been studied using spherical shape Fe_3O_4 nano particles.

Figures 2 to 4 illustrates the impact of ϕ on l',θ' and C' profiles. It is understood from the plots that l' and θ'diminishes with increase in ϕ while concentration increases. Figures 5 to 15 display the hold of diverse non-dimensional parameters on θ',l' and C' profiles. These profiles have been drawn according to the variation in z. The l' profile increases with rise in Hall current parameter (Fig.5) but velocity is diminishing with rise in M (Fig.6). Physically, the movement of ferro-nanofluid perpendicular to B_0 induces a Lorentz force against the fluid flow which retards the fluid velocity. Also, B_0 induces a Hall current which acts in the direction of the fluid flow and thus it accelerates the fluid velocity.

Concentration of ferro-nanofluid with variation in chemical reaction parameter is depicted in figures 7 and 8. The sign of chemical reaction parameter determines whether the chemical reaction is destructive or constructive [45]. It can be physically interpreted that as $K_r(K_r > 0)$

increases, a destructive chemical reaction enhances and thus concentration of the nanofluid decreases and as K_r ($K_r < 0$) decreases, a constructive chemical reaction enhances and hence concentration increases.

The profiles for l', θ' and C' of ferro-nanofluid with changes in heat source parameter are illustrated in the figures 9 to 11. It can be physically interpreted that a rise in S enhances the fluid temperature and increases the kinetic energy level in molecules of nanofluid. Consequently, l' of the ferro-nanofluid goes up and C' comes down.

l' and θ' profiles of the ferro-nanofluid with variation in injection/suction parameter are shown in figures 12 and 13. l' and θ' of the nanofluid near the oscillatory plate increases with increasing injection/suction parameter. Physically, these can be attributed to the fact that as ($\lambda > 0$) increases, heated fluid particles enter into the channel and cold fluid particles disappear from the channel increasing the velocity and temperature inside the channel. The process is reversed in the case ($\lambda < 0$). Concentration profile of ferro- nanofluid with variation in Soret number is depicted in figure 14. Concentration decreases due to the increase in S_0. A step up in S_0 indicates the enhancement in θ' difference and therefore C' is diminished. Figure 15 reveals that velocity of ferro-nanofluid increases with rise in α . Physically this is due to the effect of increased gravitational force. Figure 16 depicts the level of enhancement in velocity profile with increasing porosity parameter.

4.1 Statistical Analysis

The impact of different parameters on Cf,Nu and Sh (z = 1) are established using r (Correlation coefficient) and PE (Probable error) {described in the tables 5 to 7}. The sign of r determines the nature of relationship and the magnitude of r indicates the intensity of relationship [46]. The significance in the precision of correlation coefficient is verified using

PE of r and the correlation is said to be significant if r> 6 PE [47]. Probable error is calculated using the formula, PE = ($\frac{1-r^2}{\sqrt{n}}$) 0.6745; where n is the number of observations.

From Table 5, it is observed that Cf has high positive correlation with ϕ and N and high negative correlation with H,G_m,S,G_r and λ. All the values of $|\frac{r}{PE}|$ for Cf are greater than 6 meaning that the parameters described in the table are significant. Table 6 proposes that Nu is highly negatively correlated with ϕ and N and positively correlated with S and λ. From table 7, it can be inferred that Sh is highly positively correlated with ϕ and N and highly negatively correlated with S_0,λ,ω,t and K_r .

4.2 Regression Analysis

Regression analysis is a statistical modelling technique used to establish a relationship between a dependent and one or more independent variables. Tables 5 to 7 reflect the nature of relationship with single variable whereas in regression analysis the quantity of relationship is obtained with more than one independent variable. Cf, Nu and Sh are estimated using multiple linear regression models given by the form:

$$Cf_{est} = a + b_\phi\,\phi + b_H H + b_{G_m} G_m + b_S\,S + b_N\,N + b_{G_r} G_r + b_\lambda\,\lambda$$

$$Nu_{est} = a + b_\phi\,\phi + b_S\,S + b_N N + b_\lambda\,\lambda$$

$$Sh_{est} = a + b_\phi\,\phi + b_N\,N + b_{S_0} S_0 + b_\lambda \lambda + b_\omega\,\omega + b_t\,t + b_{K_r} K_r$$

Where a,b_ϕ,b_H,b_{G_m} ,b_S,b_N,b_{G_r},b_λ,b_{S_0},b_ω,b_t and b_{K_r} are the estimated regression coefficients. These values are estimated for the table (2-4) values using MATLAB software. It can be noted from tables 8-10 that all Sig. value <0.05 (p Value) proving that the calculated regression coefficients are significant. From tables 8 to 10 it is observed that the R-squared values are approximately equal to 1 and also error is negligibly small (close to 0) meaning that the test is effective. The estimated Cf,Nu and Sh are:

$$Cf_{est} = 0.652231 + 0.654027\,\phi - 0.043\,H - 0.017\,G_m - 0.0108\,S + 0.043069\,N - 0.03946\,G_r - 0.38702\,\lambda$$

$$Nu_{est} = 3.350136 - 28.7968\,\phi + 0.42104\,S - 1.98807\,N + 6.334471\,\lambda$$

$$Sh_{est} = 1.812674 + 5.495754\,\phi + 0.034541\,N - 1.818151\,S_0 - 0.594991\lambda - 0.001988\,\omega - 0.022729\,t - 0.111039\,K_r$$

It is understood from the regression equations that H,G_m,S,G_r and λ have a negative impact on Cf whereas N and ϕ has a positive impact on Cf. Physically, mounting values of N and ϕ create a significant increase in the values of Cf while it reverses in the case of negatively impacted parameters. These results coincide with the results described in table 5. Enhancing the value of ϕ and N diminishes the value of Nu while an increase in S and λ increases the value of Nu. These results are in perfect synchronization with the observations in Table 6. Similarly, from the regression equation for Sh, it is understood that ϕ and N have a positive impact on Sh whereas S_0,λ,ω,t and K_r have a negative impact on Sh. This is in agreement with the findings in Table 7. Figure 17 a-c illustrates the accuracy of the regression model for the chosen sample. A commendable agreement is noted between the numerically calculated values and regression values.

5. Conclusion

The influence of heat source and hall current on magneto-hydrodynamic ferro-nanoflow in an inclined porous channel with radiation and chemical reaction has been theoretically analysed. The major conclusions drawn from the current analysis are given below:

- Hall current and injection/suction parameter plays a crucial role in amplifying the velocity profile.

- The temperature and velocity profiles are directly proportional to the heat source parameter, S.
- Angle of inclination, α has a constructive effect on the velocity profiles.
- The volume fraction of the nanoparticles, ϕ enhances the concentration profiles but reduces the temperature and velocity profiles.
- Increase in Hartmann number accounts for a reduction in velocity profile.
- The Soret effect has a destructive impact on concentration profiles.
- Heat source and hall current has a negative impact on skin friction.
- An increase of 0.982513 per unit S (heat source) is noted due to the impact of heat source on Nusselt number.
- Soret number has a negative impact (a decrease of 1.853334359 per unit S_o) on Sherwood number.

Molecule transport in a slanted rectangular channel is usual in designing applications, e.g., molecule infiltration through splits of building envelopes and molecule transport in micro channels [48]. Slanted pipe and channels have extensive applications in automobile industry for designing equipment's. Nanoparticles can considerably reduce the size of equipment's and show a better performance than the existing ones. Our future aim is to extend the present study by incorporating viscous dissipation, Joule heating and entropy generations which are decisive in heat and mass transfer rates.

REFERENCES

[1] S.U.S. Choi, J.A. Eastman, Enhancing thermal conductivity of fluids with nanoparticles, in: Conf. 1995 Int. Mech. Eng. Congr. Exhib. San Fr. CA (United States), 12-17 Nov 1995, n.d.

[2] A. Chamkha, S. Jena, S. Mahapatra, MHD Convection of Nanofluids: A Review, J. Nanofluids. 4 (2015). https://doi.org/10.1166/jon.2015.1166.

[3] J.A. Eastman, U.S. Choi, S. Li, L.J. Thompson, S. Lee, Enhanced Thermal Conductivity through the Development of Nanofluids, MRS Proc. 457 (1996) 3. https://doi.org/10.1557/PROC-457-3.

[4] K.Y. Leong, I. Razali, ku zarina ku ahmad, H.C. Ong, M.J. Ghazali, A.R. Mohd Rosdzimin, Thermal conductivity of an ethylene glycol/water-based nanofluid with copper-titanium dioxide nanoparticles: An experimental approach, Int. Commun. Heat Mass Transf. 90 (2018) 23–28. https://doi.org/10.1016/j.icheatmasstransfer.2017.10.005.

[5] J. Uddin, W. Khan, A. Ismail, MHD Free Convective Boundary Layer Flow of a Nanofluid past a Flat Vertical Plate with Newtonian Heating Boundary Condition, PLoS One. 7 (2012) e49499. https://doi.org/10.1371/journal.pone.0049499.

[6] Z. Shah, S. Islam, T. Gul, E. Bonyah, M. [Altaf Khan], The electrical MHD and Hall current impact on micropolar nanofluid flow between rotating parallel plates, Results Phys. 9 (2018) 1201–1214. https://doi.org/10.1016/j.rinp.2018.01.064.

[7] M.V. Krishna, A.J. Chamkha, Hall and ion slip effects on Unsteady MHD Convective Rotating flow of Nanofluids—Application in Biomedical Engineering, J. Egypt. Math. Soc. 28 (2020) 1. https://doi.org/10.1186/s42787-019-0065-2.

[8] R. Kumar, S. Sood, Combined influence of fluctuations in the temperature and stretching velocity of the sheet on MHD flow of Cu-water nanofluid through rotating porous medium with cubic auto-catalysis chemical reaction, J. Mol. Liq. 237 (2017) 347–360. https://doi.org/10.1016/j.molliq.2017.04.054.

[9] H. Babazadeh, R. Kumar, R.N. Dara, A. Shafee, Simulation Examination for Nanoparticle Flow in a Permeable Enclosure via CVFEM Involving MHD Effect, Arab. J. Sci. Eng. (2020). https://doi.org/10.1007/s13369-020-04381-1.

[10] R. Kumar, S. Sood, Effect of quadratic density variation on mixed convection stagnation point heat transfer and MHD fluid flow in porous medium towards a permeable shrinking sheet, J. Porous Media. 19 (2016) 1083–1097. https://doi.org/10.1615/JPorMedia.v19.i12.50.

[11] S. Das, R.N. Jana, O. Makinde, Transient natural convection in a vertical channel filled with nanofluids in the presence of thermal radiation, Alexandria Eng. J. 55 (2015). https://doi.org/10.1016/j.aej.2015.10.013.

[12] M. Maghrebi, M. Nazari, T. Armaghani, Forced Convection Heat Transfer of Nanofluids in a Porous Channel, Transp. Porous Media. 93 (2012). https://doi.org/10.1007/s11242-012-9959-2.

[13] K.D.Singh, D.A. Mathew, An oscillatory free convective flow through porous medium in a rotating vertical porous channel, Global Journal of Science Frontier Research

Mathematics & Decision Sciences.12(2012)3 51-64.

[14] K.D.Singh, A. Mathew, Injection/suction effect on an oscillatory hydromagnetic flow in a rotating horizontal porous channel, Indian J. Phys. 82 (2008) 435–445.

[15] A. Zeeshan, R. Ellahi, M. Hassan, Magnetohydrodynamic flow of water/ethylene glycol based nanofluids with natural convection through a porous medium, Eur. Phys. J. Plus. 129 (2014) 261. https://doi.org/10.1140/epjp/i2014-14261-5.

[16] M. Turkyilmazoglu, Unsteady Convection Flow of Some Nanofluids Past a Moving Vertical Flat Plate With Heat Transfer, J. Heat Transfer. 136 (2013) 31704. https://doi.org/10.1115/1.4025730.

[17] E. Haile, Heat and Mass Transfer Through a Porous Media of MHD Flow of Nanofluids with Thermal Radiation, Viscous Dissipation and Chemical Reaction Effects, Am. Chem. Sci. J. 4 (2014) 828–846. https://doi.org/10.9734/ACSJ/2014/11082.

[18] P.K. Kameswaran, M. Narayana, P. Sibanda, P.V.S.N. Murthy, Hydromagnetic nanofluid flow due to a stretching or shrinking sheet with viscous dissipation and chemical reaction effects, Int. J. Heat Mass Transf. 55 (2012) 7587–7595. https://doi.org/10.1016/j.ijheatmasstransfer.2012.07.065.

[19] N. Tarakaramu, P. Narayan, Unsteady MHD nanofluid flow over a stretching sheet with chemical reaction, IOP Conf. Ser. Mater. Sci. Eng. 263 (2017) 62030. https://doi.org/10.1088/1757-899X/263/6/062030.

[20] C. Zhang, L. Zheng, X. Zhang, G. Chen, MHD flow and radiation heat transfer of nanofluids in porous media with variable surface heat flux and chemical reaction, Appl. Math. Model. 39 (2015) 165–181. https://doi.org/10.1016/j.apm.2014.05.023.

[21] R. Kumar, S. Sood, M. Sheikholeslami, S.A. Shehzad, Nonlinear thermal radiation and cubic autocatalysis chemical reaction effects on the flow of stretched nanofluid under rotational oscillations, J. Colloid Interface Sci. 505 (2017) 253–265. https://doi.org/10.1016/j.jcis.2017.05.083.

[22] K. Das, P.R. Duari, P.K. Kundu, Nanofluid flow over an unsteady stretching surface in presence of thermal radiation, Alexandria Eng. J. 53 (2014) 737–745. https://doi.org/10.1016/j.aej.2014.05.002.

[23] M.A. Hossain, H.S. Takhar, Radiation effect on mixed convection along a vertical plate with uniform surface temperature, Heat Mass Transf. 31 (1996) 243–248. https://doi.org/10.1007/BF02328616.

[24] A.A. Mohammadein, M.F. El-Amin, Thermal radiation effects on power-law fluids over a horizontal plate embedded in a porous medium, Int. Commun. Heat Mass Transf. 27 (2000) 1025–1035. https://doi.org/10.1016/S0735-1933(00)00182-2.

[25] R. Kumar, S. Sood, S.A. Shehzad, M. Sheikholeslami, Radiative heat transfer study for flow of non-Newtonian nanofluid past a Riga plate with variable thickness, J. Mol. Liq. 248 (2017) 143–152. https://doi.org/10.1016/j.molliq.2017.10.018.

[26] K. Sekhar, G. Reddy, C. Raju, B. Pullepu, R. Kumar, S. Shehzad, Aligned magnetic dipole in nonlinear radiative Falkner-Skan flow of Casson fluid over a wedge containing suspension of nanoparticles and microorganisms, Int. J. Nanoparticles. 9 (2017) 213. https://doi.org/10.1504/IJNP.2017.089447.

[27] P. Ram, H. Singh, R. Kumar, V. Kumar, V. Joshi, Free Convective Boundary Layer Flow of Radiating and Reacting MHD Fluid Past a Cosinusoidally Fluctuating Heated Plate, Int. J. Appl. Comput. Math. 3 (2017). https://doi.org/10.1007/s40819-017-0355-z.

[28] D. Pal, B. Talukdar, Influence of Hall Current and Thermal Radiation on MHD Convective Heat and Mass Transfer in a Rotating Porous Channel with Chemical Reaction, Int. J. Eng. Math. 2013 (2013) 367064. https://doi.org/10.1155/2013/367064.

[29] P. Sulochana, Hall Effects on Unsteady MHD Three Dimensional Flow through a Porous Medium in a Rotating Parallel Plate Channel with Effect of Inclined Magnetic Field, Am. J. Comput. Math. 04 (2014) 396–405. https://doi.org/10.4236/ajcm.2014.45034.

[30] S.M. Ibrahim, K. Suneetha, Heat source and chemical effects on MHD convection flow embedded in a porous medium with Soret, viscous and Joules dissipation, Ain Shams Eng. J. 7 (2016) 811–818. https://doi.org/10.1016/j.asej.2015.12.008.

[31] M. Turkyilmazoglu, I. Pop, Soret and heat source effects on the unsteady radiative MHD free convection flow from an impulsively started infinite vertical plate, Int. J. Heat Mass Transf. 55 (2012) 7635–7644. https://doi.org/10.1016/j.ijheatmasstransfer.2012.07.079.

[32] M.S. Malashetty, J.C. Umavathi, Two-phase magnetohydrodynamic flow and heat transfer in an inclined channel, Int. J. Multiph. Flow. 23 (1997) 545–560. https://doi.org/10.1016/S0301-9322(96)00068-7.

[33] S. Said, M.A. Habib, H. Badr, S. Anwar, Numerical investigation of natural convection inside an inclined parallel-walled channel, Int. J. Numer. Methods Fluids. 49 (2005) 569–582. https://doi.org/10.1002/fld.1013.

[34] J. Hasnain, Z. Abbas, M. Sajid, Effects of Porosity and Mixed Convection on MHD Two Phase Fluid Flow in an Inclined Channel, PLoS One. 10 (2015) e0119913. https://doi.org/10.1371/journal.pone.0119913.

[35] S. Hussain, K. Mehmood, M. Sagheer, A. Farooq, Entropy generation analysis of mixed convective flow in an inclined channel with cavity with Al 2 O 3 -water nanofluid in porous medium, Int. Commun. Heat Mass Transf. 89 (2017) 198–210. https://doi.org/10.1016/j.icheatmasstransfer.2017.10.009.

[36] R.L. Hamilton, O.K. Crosser, Thermal Conductivity of Heterogeneous Two-Component Systems, Ind. Eng. Chem. Fundam. 1 (1962) 187–191. https://doi.org/10.1021/i160003a005.

[37] P. Balvinder, D. Krishan, A.K. Bansal, Hall current effect on viscoelastic (Walter's liquid model-B) MHD oscillatory convective channel flow through a porous medium with heat radiation, Kragujev. J. Sci. 36 (2014) 19–32. https://doi.org/10.5937/KgJSci1436019B.

[38] S. Sureshkumar, M. Muthtamilselvan, A slanted porous enclosure filled with Cu-water nanofluid, Eur. Phys. J. Plus. 131 (2016) 95. https://doi.org/10.1140/epjp/i2016-16095-5.

[39] O.D. Makinde, I.L. Animasaun, Bioconvection in {MHD} nanofluid flow with nonlinear thermal radiation and quartic autocatalysis chemical reaction past an upper surface of a paraboloid of revolution, Int. J. Therm. Sci. 109 (2016) 159–171.

https://doi.org/10.1016/j.ijthermalsci.2016.06.003.

[40] D.P. Telionis, Unsteady Viscous Flows, Springer-Verlag, 1981. https://books.google.co.in/books?id=9FiqAAAAIAAJ.

[41] P.K. Sharma, B.K. Sharma, R.C. Chaudhary, Unsteady free covection oscillatory couette flow through a porous medium with periodic wall temperature, Tamkang J. Math. 38 (2007) 93–102. https://doi.org/10.5556/j.tkjm.38.2007.97.

[42] M. Sheikholeslami, D.D. Ganji, Ferrohydrodynamic and magnetohydrodynamic effects on ferrofluid flow and convective heat transfer, Energy. 75 (2014) 400–410. https://doi.org/10.1016/j.energy.2014.07.089.

[43] R. Kumar, R. Kumar, S. [Ali Shehzad], M. Sheikholeslami, Rotating frame analysis of radiating and reacting ferro-nanofluid considering Joule heating and viscous dissipation, Int. J. Heat Mass Transf. 120 (2018) 540–551. https://doi.org/10.1016/j.ijheatmasstransfer.2017.12.069.

[44] H. Aminfar, M. Mohammadpourfard, F. Mohseni, Two-phase mixture model simulation of the hydro-thermal behavior of an electrical conductive ferrofluid in the presence of magnetic fields, J. Magn. Magn. Mater. 324 (2012) 830–842. https://doi.org/10.1016/j.jmmm.2011.09.028.

[45] D. Sarma, K.K. Pandit, Effects of Hall current, rotation and Soret effects on MHD free convection heat and mass transfer flow past an accelerated vertical plate through a porous medium, Ain Shams Eng. J. 9 (2018) 631–646. https://doi.org/10.1016/j.asej.2016.03.005.

[46] J. Mackolil, B. Mahanthesh, Exact and statistical computations of radiated flow of nano and Casson fluids under heat and mass flux conditions, J. Comput. Des. Eng. 6 (2019) 593–605. https://doi.org/10.1016/j.jcde.2019.03.003.

[47] R.A. FISHER, On the “probable error” of a coefficient of correlation deduced from a small sample, Metron. 1 (1921) 1–32. https://ci.nii.ac.jp/naid/10012392243/en/.

[48] Y. Gao, Y. Yu, K. Zhong, Y. Kang, Analytical solutions for particle transport through an inclined channel with gravitational effect, Chinese J. Phys. 60 (2019) 180–192. https://doi.org/10.1016/j.cjph.2019.05.010.

Appendix

$$\eta_1 = \frac{\phi_4\lambda + \sqrt{(\phi_4\lambda)^2 - 4\lambda_n \frac{(-N^2+S)}{(P_r)^2}}}{2\left(\frac{\lambda_n}{P_r}\right)} \qquad \eta_2 = \frac{\phi_4\lambda - \sqrt{(\phi_4\lambda)^2 - 4\lambda_n \frac{(-N^2+S)}{(P_r)^2}}}{2\left(\frac{\lambda_n}{P_r}\right)}$$

$$\eta_3 = \frac{\phi_4\lambda + \sqrt{(\phi_4\lambda)^2 - 4\frac{\lambda_n}{P_r}\left(\frac{S}{P_r} - \frac{N^2}{P_r} - \omega i\phi_4\right)}}{2\left(\frac{\lambda_n}{P_r}\right)} \qquad \eta_4 = \frac{\phi_4\lambda - \sqrt{(\phi_4\lambda)^2 - 4\frac{\lambda_n}{P_r}\left(\frac{S}{P_r} - \frac{N^2}{P_r} - \omega i\phi_4\right)}}{2\left(\frac{\lambda_n}{P_r}\right)}$$

$$\eta_5 = \frac{\phi_4\lambda + \sqrt{(\phi_4\lambda)^2 - 4\frac{\lambda_n}{P_r}\left(\frac{S}{P_r} - \frac{N^2}{P_r} + \omega i\phi_4\right)}}{2\left(\frac{\lambda_n}{P_r}\right)} \qquad \eta_6 = \frac{\phi_4\lambda - \sqrt{(\phi_4\lambda)^2 - 4\frac{\lambda_n}{P_r}\left(\frac{S}{P_r} - \frac{N^2}{P_r} + \omega i\phi_4\right)}}{2\left(\frac{\lambda_n}{P_r}\right)}$$

$$q_1 = \frac{\lambda + \sqrt{\lambda^2 + 4K_r\frac{\lambda^2}{S_c}}}{\frac{2}{S_c}} \qquad q_2 = \frac{\lambda - \sqrt{\lambda^2 + 4K_r\frac{\lambda^2}{S_c}}}{\frac{2}{S_c}} \qquad q_3 = \frac{\lambda + \sqrt{\lambda^2 + \frac{4}{S_c}(K_r\lambda^2 + \omega i)}}{\frac{2}{S_c}}$$

$$q_4 = \frac{\lambda - \sqrt{\lambda^2 + \frac{4}{S_c}(K_r\lambda^2 + \omega i)}}{\frac{2}{S_c}} \qquad q_5 = \frac{\lambda + \sqrt{\lambda^2 + \frac{4}{S_c}(K_r\lambda^2 - \omega i)}}{\frac{2}{S_c}}$$

$$q_6 = \frac{\lambda - \sqrt{\lambda^2 + \frac{4}{S_c}(K_r\lambda^2 - \omega i)}}{\frac{2}{S_c}} \qquad \chi_1 = \frac{\phi_1\lambda + \sqrt{(\phi_1\lambda)^2 + 4\phi_2 p'}}{2\phi_2}$$

$$\chi_2 = \frac{\phi_1\lambda - \sqrt{(\phi_1\lambda)^2 + 4\phi_2 p'}}{2\phi_2} \qquad \chi_3 = \frac{\phi_1\lambda + \sqrt{(\phi_1\lambda)^2 + 4\phi_2 q'}}{2\phi_2}$$

$$\chi_4 = \frac{\phi_1\lambda - \sqrt{(\phi_1\lambda)^2 + 4\phi_2 q'}}{2\phi_2} \qquad \chi_5 = \frac{\phi_1\lambda + \sqrt{(\phi_1\lambda)^2 + 4\phi_2 r'}}{2\phi_2}$$

$$\chi_6 = \frac{\phi_1\lambda - \sqrt{(\phi_1\lambda)^2 + 4\phi_2 r'}}{2\phi_2} \qquad A_{11} = \frac{-S_0(\eta_1)^2 m_1}{\frac{1}{S_c}(\eta_1)^2 - \lambda\eta_1 - K_r\lambda^2}$$

$$A_{12} = \frac{-S_0(\eta_2)^2 m_2}{\frac{1}{S_c}(\eta_2)^2 - \lambda\eta_2 - K_r\lambda^2} \qquad A_{21} = \frac{-S_0(\eta_3)^2 m_3}{\frac{1}{S_c}(\eta_3)^2 - \lambda\eta_3 - (K_r\lambda^2 + \omega i)}$$

$$A_{22} = \frac{-S_0(\eta_4)^2 m_4}{\frac{1}{S_c}(\eta_4)^2 - \lambda\eta_4 - (K_r\lambda^2 + \omega i)} \qquad A_{31} = \frac{-S_0(\eta_5)^2 m_5}{\frac{1}{S_c}(\eta_5)^2 - \lambda\eta_5 + (-K_r\lambda^2 + \omega i)}$$

$$A_{32} = \frac{-S_0(\eta_6)^2 m_6}{\frac{1}{S_c}(\eta_6)^2 - \lambda\eta_6 + (-K_r\lambda^2 + \omega i)} \qquad D_{11} = 1 \qquad D_{12} = \frac{-\phi_3 G_r(\lambda)^2 m_1 sin\alpha}{\phi_2(\eta_1)^2 - \phi_1\lambda\eta_1 - p'}$$

$$D_{13} = \frac{-\phi_3 G_r(\lambda)^2 m_2 sin\alpha}{\phi_2(\eta_2)^2 - \phi_1\lambda\eta_2 - p'} \qquad D_{14} = \frac{-\phi_3 G_m(\lambda)^2 \zeta_1 sin\alpha}{\phi_2(q_1)^2 - \phi_1\lambda q_1 - p'}$$

$$D_{15} = \frac{-\phi_3 G_m(\lambda)^2 \zeta_2 sin\alpha}{\phi_2(q_2)^2 - \phi_1\lambda q_2 - p'} \qquad D_{16} = \frac{-\phi_3 G_m(\lambda)^2 A_{11} sin\alpha}{\phi_2(\eta_1)^2 - \phi_1\lambda\eta_1 - p'}$$

$$D_{17} = \frac{-\phi_3 G_m(\lambda)^2 A_{12} sin\alpha}{\phi_2(\eta_2)^2 - \phi_1\lambda\eta_2 - p'} \qquad D_{21} = 1 \qquad D_{22} = \frac{-\phi_3 G_r(\lambda)^2 m_3 sin\alpha}{\phi_2(\eta_3)^2 - \phi_1\lambda\eta_3 - q'}$$

$$D_{23} = \frac{-\phi_3 G_r(\lambda)^2 m_4 sin\alpha}{\phi_2(\eta_4)^2 - \phi_1\lambda\eta_4 - q'} \qquad D_{24} = \frac{-\phi_3 G_m(\lambda)^2 \zeta_3 sin\alpha}{\phi_2(q_3)^2 - \phi_1\lambda q_3 - q'}$$

$$D_{25} = \frac{-\phi_3 G_m(\lambda)^2 \zeta_4 sin\alpha}{\phi_2(q_4)^2 - \phi_1\lambda q_4 - q'} \qquad D_{26} = \frac{-\phi_3 G_m(\lambda)^2 A_{21} sin\alpha}{\phi_2(\eta_3)^2 - \phi_1\lambda\eta_3 - q'}$$

$$D_{27} = \frac{-\phi_3 G_m(\lambda)^2 A_{22} sin\alpha}{\phi_2(\eta_4)^2 - \phi_1\lambda\eta_4 - q'} \qquad D_{31} = 1 \qquad D_{32} = \frac{-\phi_3 G_r(\lambda)^2 m_5 sin\alpha}{\phi_2(\eta_5)^2 - \phi_1\lambda\eta_5 - r'}$$

$$D_{33} = \frac{-\phi_3 G_r(\lambda)^2 m_6 sin\alpha}{\phi_2(\eta_6)^2 - \phi_1\lambda\eta_6 - r'} \qquad D_{34} = \frac{-\phi_3 G_m(\lambda)^2 \zeta_5 sin\alpha}{\phi_2(q_5)^2 - \phi_1\lambda q_5 - r'}$$

$$D_{35} = \frac{-\phi_3 G_m(\lambda)^2 \zeta_6 sin\alpha}{\phi_2(q_6)^2 - \phi_1\lambda q_6 - r'} \qquad D_{36} = \frac{-\phi_3 G_m(\lambda)^2 A_{31} sin\alpha}{\phi_2(\eta_5)^2 - \phi_1\lambda\eta_5 - r'}$$

$$D_{37} = \frac{-\phi_3 G_m(\lambda)^2 A_{32} sin\alpha}{\phi_2(\eta_6)^2 - \phi_1\lambda\eta_6 - r'} \qquad m_1 = \frac{-\mathrm{e}^{(\eta_2)}}{e^{(\eta_1)} - \mathrm{e}^{(\eta_2)}} \qquad m_2 = 1 - m_1 \qquad m_3 = \frac{-\mathrm{e}^{(\eta_4)}}{e^{(\eta_3)} - \mathrm{e}^{(\eta_4)}}$$

$$m_4 = 1 - m_3 \qquad m_5 = \frac{-e^{(\eta_6)}}{e^{(\eta_5)} - e^{(\eta_6)}} \qquad m_6 = 1 - m_5$$

$$\zeta_1 = \frac{e^{(q_2)} - A_{11}\left(e^{(q_2)} - e^{(\eta_1)}\right) + A_{12}\left(e^{(\eta_2)} - e^{(q_2)}\right)}{e^{(q_2)} - e^{(q_1)}} \qquad \zeta_2 = 1 - \zeta_1 - A_{11} - A_{12}$$

$$\zeta_3 = \frac{e^{(q_4)} - A_{21}\left(e^{(q_4)} - e^{(\eta_3)}\right) + A_{22}\left(e^{(\eta_4)} - e^{(q_4)}\right)}{e^{(q_4)} - e^{(q_3)}} \qquad \zeta_4 = 1 - \zeta_3 - A_{21} - A_{22}$$

$$\zeta_5 = \frac{e^{(q_6)} - A_{31}\left(e^{(q_6)} - e^{(\eta_5)}\right) + A_{32}\left(e^{(\eta_6)} - e^{(q_6)}\right)}{e^{(q_6)} - e^{(q_5)}} \qquad \zeta_6 = 1 - \zeta_5 - A_{31} - A_{32}$$

$$h_1 = \frac{\begin{array}{r} -1 + \mathrm{D}_{11}(1 - \mathrm{e}^{(\chi_2)}) - D_{12}\left(e^{(\chi_2)} - e^{(\eta_1)}\right) \\ - D_{13}\left(e^{(\chi_2)} - e^{(\eta_2)}\right) + D_{14}\left(e^{(q_1)} - e^{(\chi_2)}\right) + D_{15}\left(e^{(q_2)} - e^{(\chi_2)}\right) \\ + D_{16}\left(e^{(\eta_1)} - e^{(\chi_2)}\right) + D_{17}\left(e^{(\eta_2)} - e^{(\chi_2)}\right) \end{array}}{e^{(\chi_2)} - e^{(\chi_1)}}$$

$$h_2 = -h_1 - D_{11} - D_{12} - D_{13} - D_{14} - D_{15} - D_{16} - D_{17}$$

$$h_3 = \frac{\begin{array}{r} -1 + D_{21}(1 - e^{(\chi_4)}) - D_{22}(e^{(\chi_4)} - e^{(\eta_3)}) \\ - D_{23}(e^{(\chi_4)} - e^{(\eta_4)}) + D_{24}(e^{(q_3)} - e^{(\chi_4)}) + D_{25}(e^{(q_4)} - e^{(\chi_4)}) \\ + D_{26}(e^{(\eta_3)} - e^{(\chi_4)}) + D_{27}(e^{(\eta_4)} - e^{(\chi_4)}) \end{array}}{e^{(\chi_4)} - e^{(\chi_3)}}$$

$$h_4 = -h_3 - D_{21} - D_{22} - D_{23} - D_{24} - D_{25} - D_{26} - D_{27}$$

$$h_5 = \frac{\begin{array}{r} -1 + D_{31}(1 - e^{(\chi_6)}) - D_{32}(e^{(\chi_6)} - e^{(\eta_5)}) \\ - D_{33}(e^{(\chi_6)} - e^{(\eta_6)}) + D_{34}(e^{(q_5)} - e^{(\chi_6)}) + D_{35}(e^{(q_6)} - e^{(\chi_6)}) \\ + D_{36}(e^{(\eta_5)} - e^{(\chi_6)}) + D_{37}(e^{(\eta_6)} - e^{(\chi_6)}) \end{array}}{e^{(\chi_6)} - e^{(\chi_5)}}$$

$$h_6 = -h_5 - D_{31} - D_{32} - D_{33} - D_{34} - D_{35} - D_{36} - D_{37}$$

$$p' = \frac{\phi_2}{K_1} + \frac{\phi_5 M^2}{1 + H^2} + \frac{\phi_5 M^2 iH}{1 + H^2} \qquad q' = \frac{\phi_2}{K_1} + \frac{\phi_5 M^2}{1 + H^2} + \frac{\phi_5 M^2 iH}{1 + H^2} + \phi_1 \omega i$$

$$r' = \frac{\phi_2}{K_1} + \frac{\phi_5 M^2}{1 + H^2} + \frac{\phi_5 M^2 iH}{1 + H^2} - \phi_1 \omega i$$

Appendix A (Figures)

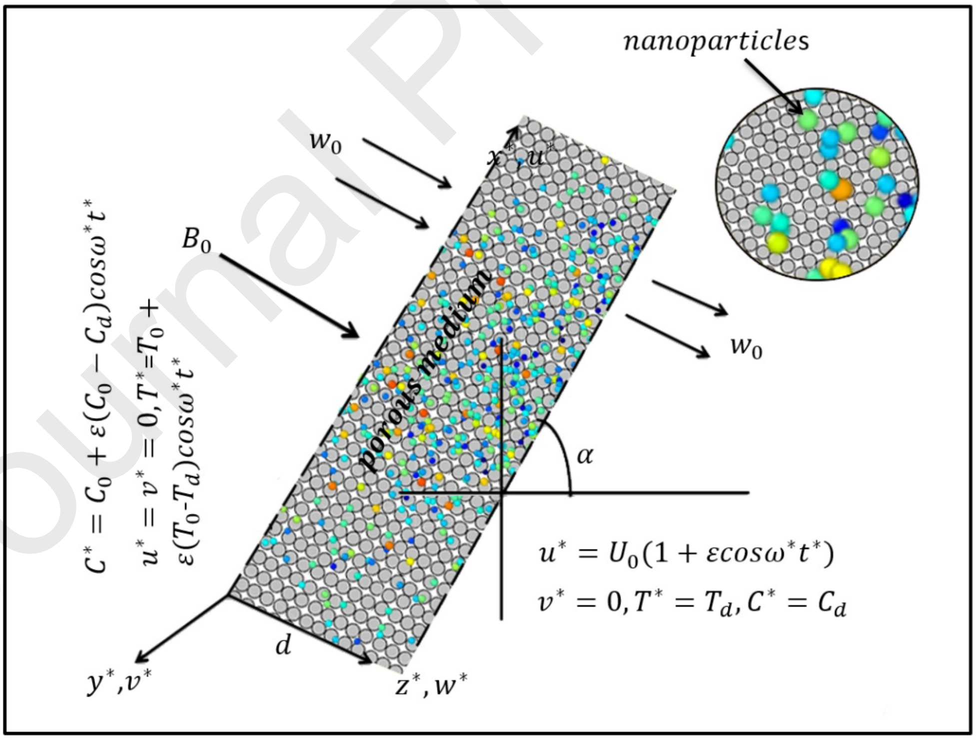

Fig.1: Physical configuration of the problem

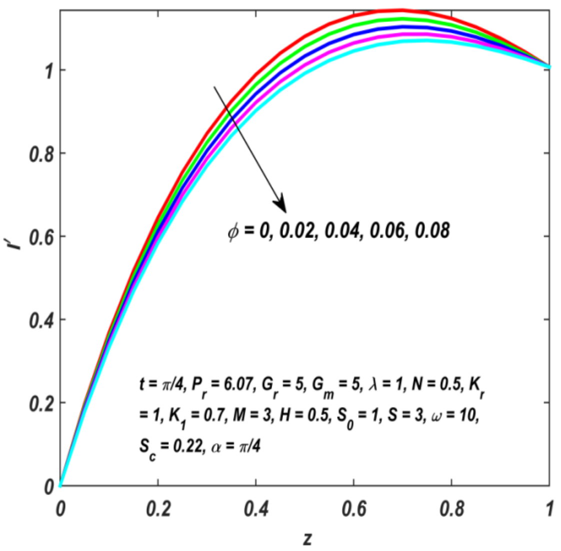

Fig.2: Variations in Velocity $l'$with ϕ

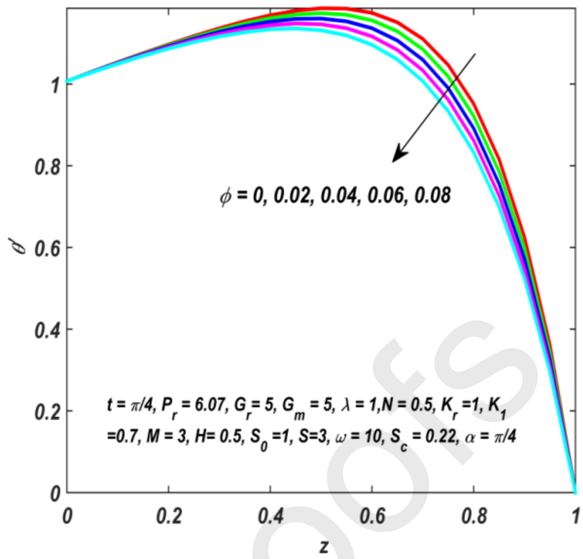

Fig.3: Variations in temperature θ' with ϕ

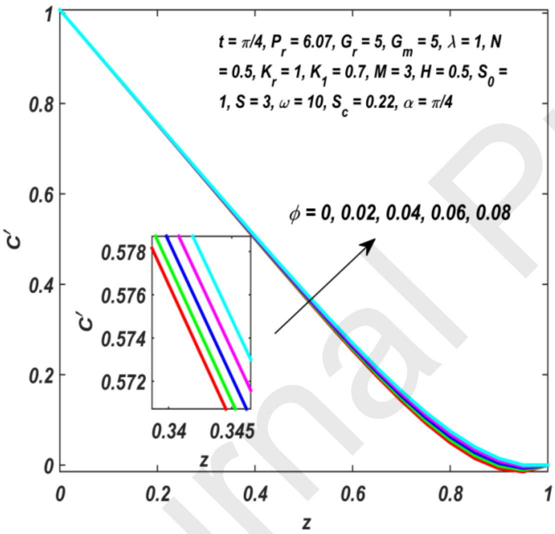

Fig.4: Variations in concentration C' with ϕ

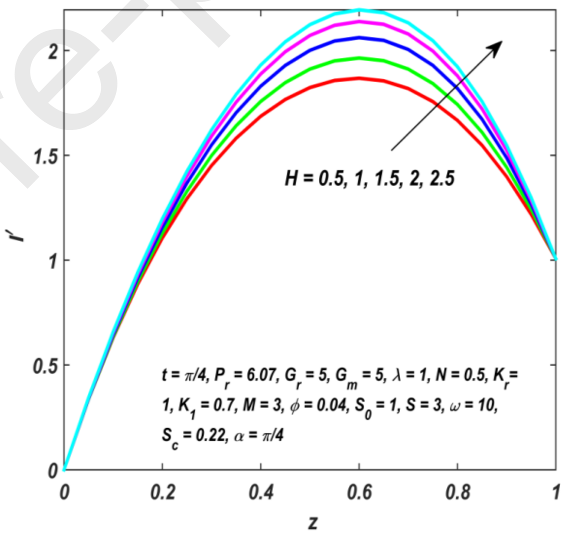

Fig.5: Variations in velocity l' with H

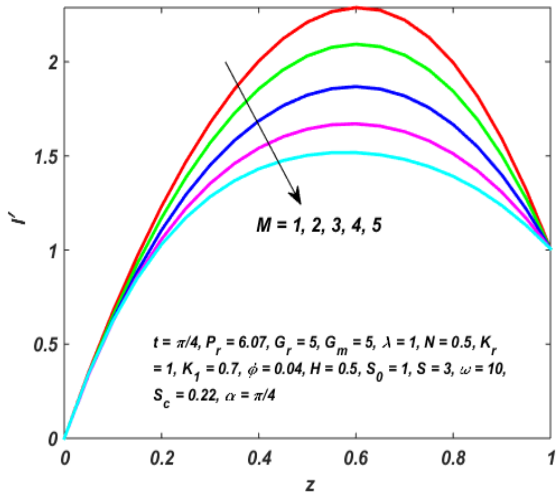

Fig.6: Variations in velocity $l'$with M

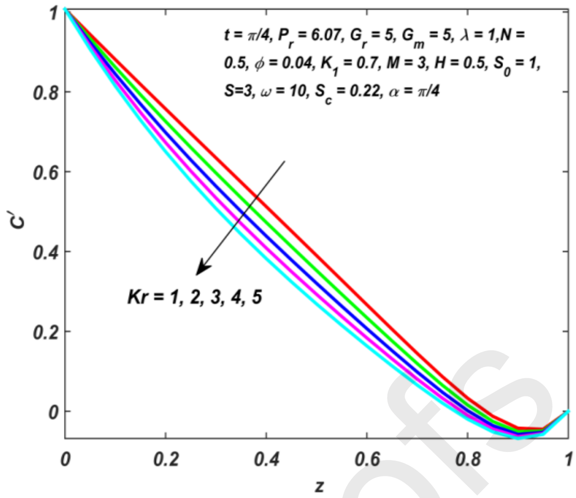

Fig.7: Variations in concentration C' with $K_r > 0$

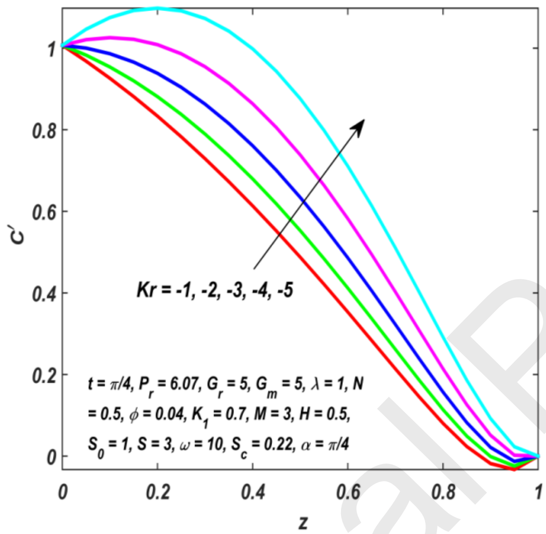

Fig.8: Variations in concentration $C'$with $(K_r < 0)$

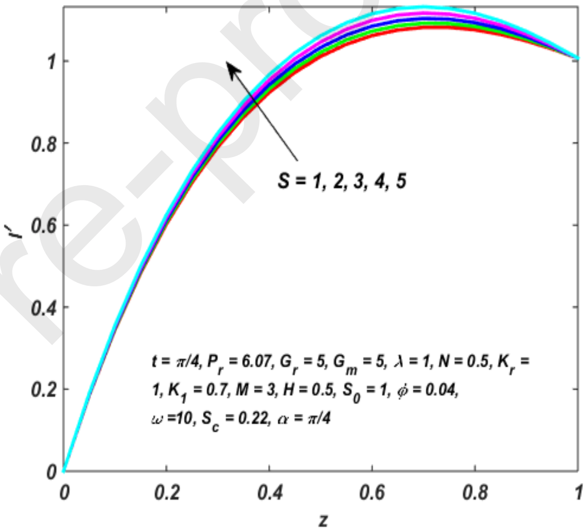

Fig.9: Variations in velocity l' with S

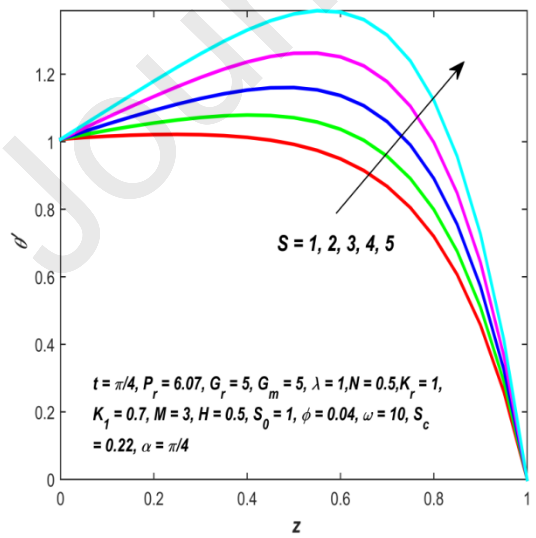

Fig.10: Variations in temperature $\theta'$with S

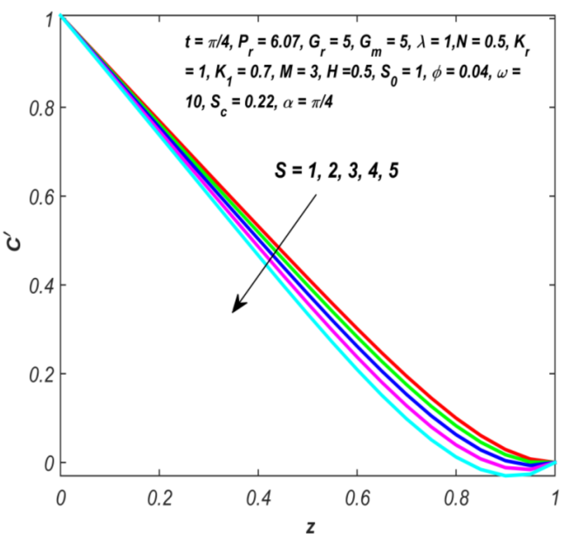

Fig.11: Variations in concentration C' with S

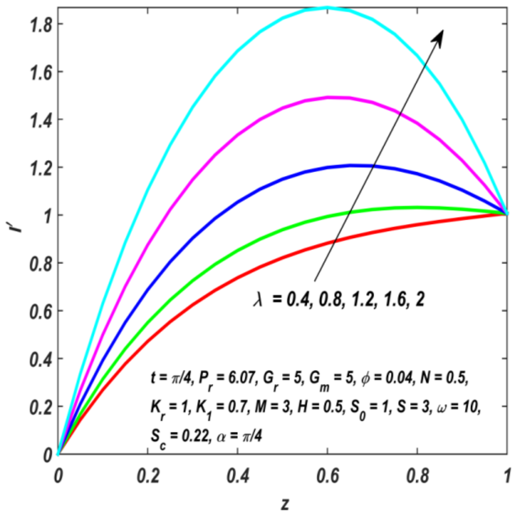

Fig.12: Variations in velocity l' with λ

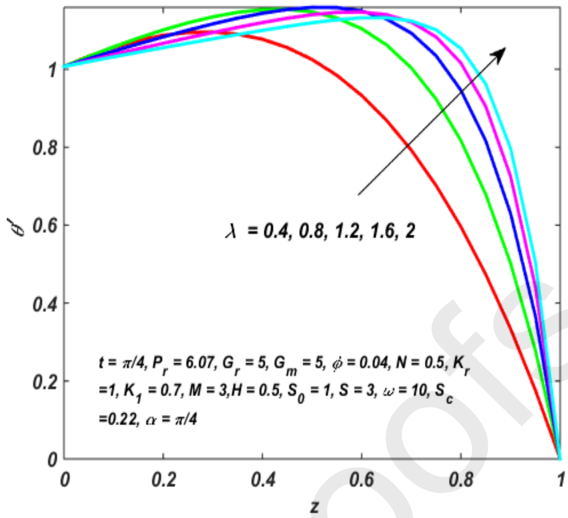

Fig.13: Variations in temperature θ' with λ

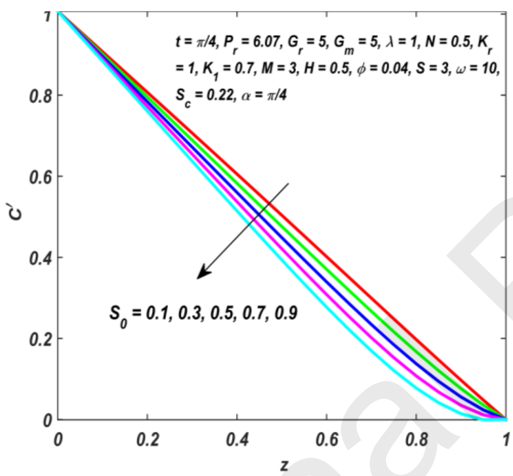

Fig.14: Variations in concentration C' with S_0

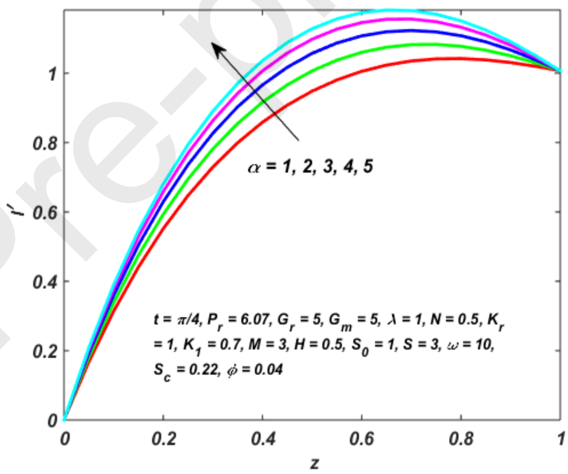

Fig.15: Variations in velocity l' with α

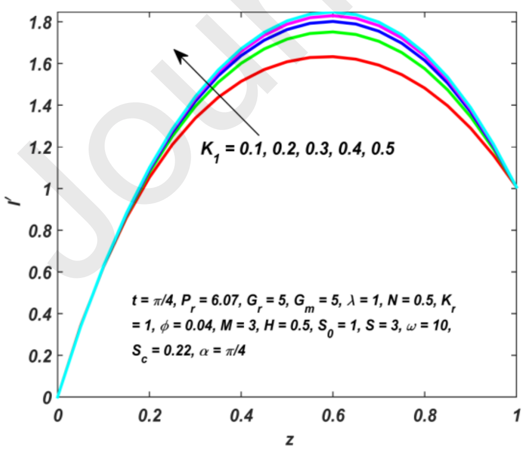

Fig.16: Variations in velocity l' with K_1

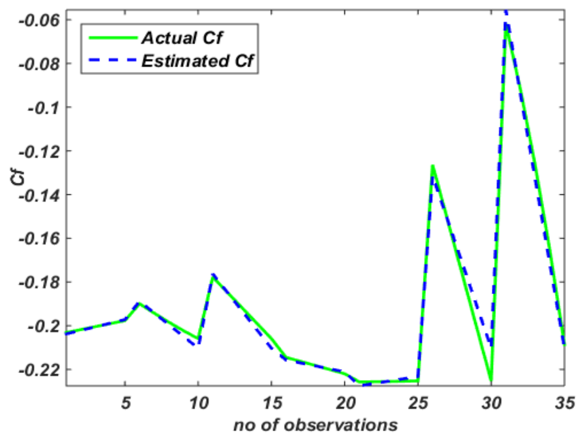

Fig.17a: Actual and estimated values of Cf

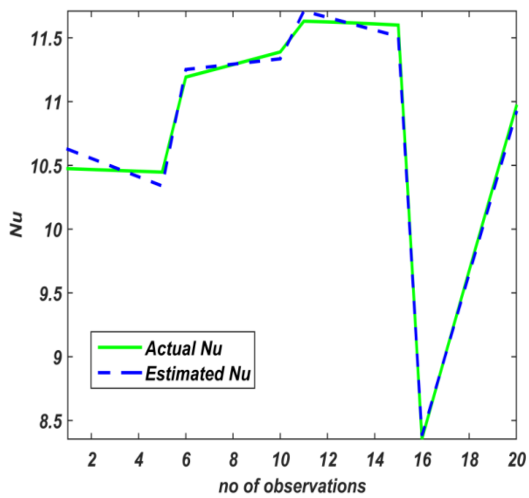

Fig.17b: Actual and estimated values of Nu

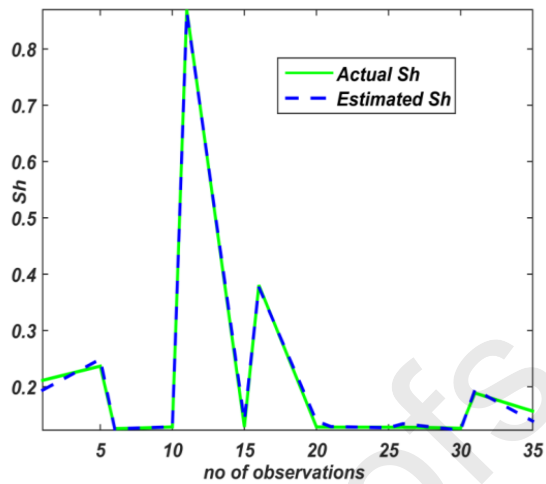

Fig.17c: Actual and estimated values of Sh

Appendix B (Tables)

Table 1. Thermo physical properties of base fluid and nanoparticles at 25^0

Model	$\rho(Kgm^{-3})$	$C_p(JKg^{-1}K^{-1})$	$k(Wm^{-1}K^{-1})$	$\beta \times 10^{-5}(K^{-1})$	$\sigma(s/m)$
Water	997.1	4179	0.613	21	0.05
Fe_3O_4	5180	670	9.7	1.3	25000

Table 2. The Skin friction of Fe_3O_4-water nanofluid when $t = \frac{\pi}{4}, P_r = 6.07, K_r = 1.5, K_1$

ϕ	H	G_m	S	N	G_r	λ	$-Cf$	Enhancement/ Decrement rate (%)
0.05	1.5	5	2	0.5	5	1.4	0.203108111	
0.0525	1.5	5	2	0.5	5	1.4	0.201751152	-0.668
0.055	1.5	5	2	0.5	5	1.4	0.200389459	-0.675
0.0575	1.5	5	2	0.5	5	1.4	0.199023038	-0.682
0.06	1.5	5	2	0.5	5	1.4	0.197651889	-0.689
Slope							-0.54562232	
0.04	1	5	2	0.5	5	1.4	0.189942907	
0.04	1.125	5	2	0.5	5	1.4	0.194262629	2.274
0.04	1.25	5	2	0.5	5	1.4	0.198388724	2.124
0.04	1.375	5	2	0.5	5	1.4	0.202275413	1.959
0.04	1.5	5	2	0.5	5	1.4	0.20589929	1.792
Slope							0.03194044	
0.04	1.5	3	2	0.5	5	1.4	0.177751404	
0.04	1.5	3.5	2	0.5	5	1.4	0.184788376	3.959
0.04	1.5	4	2	0.5	5	1.4	0.191825347	3.808
0.04	1.5	4.5	2	0.5	5	1.4	0.198862319	3.668
0.04	1.5	5	2	0.5	5	1.4	0.20589929	3.539
Slope							0.014073943	
0.04	1.5	5	2.5	0.5	5	1.4	0.214495149	
0.04	1.5	5	2.625	0.5	5	1.4	0.216330949	0.856
0.04	1.5	5	2.75	0.5	5	1.4	0.218190236	0.859
0.04	1.5	5	2.875	0.5	5	1.4	0.220073412	0.863
0.04	1.5	5	3	0.5	5	1.4	0.221980887	0.867
Slope							0.014971151	
0.04	1.5	5	2	0.1	5	1.4	0.22571289	
0.04	1.5	5	2	0.125	5	1.4	0.225624356	-0.039
0.04	1.5	5	2	0.15	5	1.4	0.225516217	-0.048
0.04	1.5	5	2	0.175	5	1.4	0.225388517	-0.057
0.04	1.5	5	2	0.2	5	1.4	0.225241303	-0.065
Slope							-0.004716052	
0.04	1.5	5	2	0.5	3	1.4	0.126386072	
0.04	1.5	5	2	0.5	3.5	1.4	0.15109988	19.554
0.04	1.5	5	2	0.5	4	1.4	0.175813688	16.356
0.04	1.5	5	2	0.5	4.5	1.4	0.200527496	14.057
0.04	1.5	5	2	0.5	5	1.4	0.225241303	12.324
Slope							0.049427616	
0.04	1.5	5	2	0.5	5	1	0.061783952	
0.04	1.5	5	2	0.5	5	1.1	0.092068285	49.017
0.04	1.5	5	2	0.5	5	1.2	0.126548023	37.450
0.04	1.5	5	2	0.5	5	1.3	0.165346706	30.659
0.04	1.5	5	2	0.5	5	1.4	0.208586679	26.151
Slope							0.366883875	

Table 3. The Nusselt number of Fe_3O_4-water nanofluid when $t = \frac{\pi}{4}, P_r = 6.07, G_r = 5, G_m = 5, K_r = 1.5, K_1 = 0.7, M = 3.5, H = 1.5, S_0 = 0.5, \omega = 20, S_c = 0.22, \alpha = \frac{\pi}{4}, R_e = 10.$

ϕ	S	N	λ	Nu	Enhancement/ Decrement rate (%)
0.05	2	0.5	1.4	10.47453	
0.0525	2	0.5	1.4	10.46772	-0.065
0.055	2	0.5	1.4	10.4609	-0.065
0.0575	2	0.5	1.4	10.45407	-0.065
0.06	2	0.5	1.4	10.44724	-0.065
Slope				-2.72878	
0.04	2.8	0.5	1.4	11.1924	
0.04	2.85	0.5	1.4	11.24113	0.435
0.04	2.9	0.5	1.4	11.29012	0.436
0.04	2.95	0.5	1.4	11.33938	0.436
0.04	3	0.5	1.4	11.3889	0.437
Slope				0.982513	
0.04	2	0.1	1.4	11.6304	
0.04	2	0.125	1.4	11.62467	-0.049
0.04	2	0.15	1.4	11.61767	-0.060
0.04	2	0.175	1.4	11.6094	-0.071
0.04	2	0.2	1.4	11.59987	-0.082
Slope				-0.30535	
0.04	2	0.5	1	8.354338	
0.04	2	0.5	1.1	9.018292	7.947
0.04	2	0.5	1.2	9.673948	7.270
0.04	2	0.5	1.3	10.32214	6.700
0.04	2	0.5	1.4	10.96381	6.216
Slope				6.5228	

$= 0.7,\ M =$ 3.5, $H = 1.5,\ S = 2, S_c = 0.22,\ \alpha = \frac{\ }{4}$.

ϕ	N	S_0	λ	ω	t	K_r	Sh	Enhancement Decrement rate (%)
0.05	0.5	0.5	1.4	20	0.785	1	0.211354922	
0.0525	0.5	0.5	1.4	20	0.785	1	0.217719958	3.012
0.055	0.5	0.5	1.4	20	0.785	1	0.224033978	2.900
0.0575	0.5	0.5	1.4	20	0.785	1	0.230297526	2.796
0.06	0.5	0.5	1.4	20	0.785	1	0.236511137	2.698
Slope							2.515599876	
0.04	0.1	0.5	1.4	20	0.785	1	0.125636143	
0.04	0.125	0.5	1.4	20	0.785	1	0.126175548	0.429
0.04	0.15	0.5	1.4	20	0.785	1	0.126834342	0.522
0.04	0.175	0.5	1.4	20	0.785	1	0.12761224	0.613
0.04	0.2	0.5	1.4	20	0.785	1	0.128508904	0.703
Slope							0.028728856	
0.04	0.5	0.1	1.4	20	0.785	1	0.869842648	
0.04	0.5	0.2	1.4	20	0.785	1	0.684509212	-21.307
0.04	0.5	0.3	1.4	20	0.785	1	0.499175776	-27.075
0.04	0.5	0.4	1.4	20	0.785	1	0.31384234	-37.128
0.04	0.5	0.5	1.4	20	0.785	1	0.128508904	-59.053
Slope							-1.853334359	
0.04	0.5	0.5	1	20	0.785	1	0.380384375	
0.04	0.5	0.5	1.1	20	0.785	1	0.317609148	-16.503
0.04	0.5	0.5	1.2	20	0.785	1	0.254751745	-19.791
0.04	0.5	0.5	1.3	20	0.785	1	0.191743117	-24.733
0.04	0.5	0.5	1.4	20	0.785	1	0.128508904	-32.979
Slope							-0.629616971	
0.04	0.5	0.5	1.4	25	0.785	1	0.128129298	
0.04	0.5	0.5	1.4	25.25	0.785	1	0.128107586	-0.017
0.04	0.5	0.5	1.4	25.5	0.785	1	0.128085347	-0.017
0.04	0.5	0.5	1.4	25.75	0.785	1	0.128062563	-0.018
0.04	0.5	0.5	1.4	26	0.785	1	0.128039217	-0.018
Slope							-9.00737E-05	
0.04	0.5	0.5	1.4	20	1	1	0.127985908	
0.04	0.5	0.5	1.4	20	1.125	1	0.127745961	-0.187
0.04	0.5	0.5	1.4	20	1.25	1	0.12735648	-0.305
0.04	0.5	0.5	1.4	20	1.375	1	0.126823545	-0.418
0.04	0.5	0.5	1.4	20	1.5	1	0.12615547	-0.527
Slope							-0.003666633	
0.04	0.5	0.5	1.4	20	0.785	0.5	0.188845397	
0.04	0.5	0.5	1.4	20	0.785	0.625	0.180650674	-4.339
0.04	0.5	0.5	1.4	20	0.785	0.75	0.172561791	-4.478
0.04	0.5	0.5	1.4	20	0.785	0.875	0.164576994	-4.627
0.04	0.5	0.5	1.4	20	0.785	1	0.156694567	-4.790
Slope							-0.064300271	

Table 5. Correlation coefficient (r), Probable error (PE) and $|\frac{r}{PE}|$ values of Cf with respect to the parameters ϕ,H,G_m ,S,N,G_r and λ

Parameter	r	PE	$\lvert\frac{r}{PE}\rvert$
ϕ	0.999997896	1.2692E-06	787896.2218
H	-0.99940294	0.000360093	2775.399238
G_m	-1	0	Inf
S	-0.999971478	1.72069E-05	58114.63519
N	0.995217965	0.002878061	345.7945854
G_r	-1	1.33958E-16	7.46505E+15
λ	-0.997583808	0.001455906	685.1977823

Table 6. Correlation coefficient (r), Probable error (PE) and $|\frac{r}{PE}|$ values of Nu with respect to the parameters ϕ,S,N and λ

parameter	r	PE	$\lvert\frac{r}{PE}\rvert$
ϕ	-0.999999812	1.13181E-07	8835395.319
S	0.999994883	3.08676E-06	323962.1929
N	-0.995220189	0.002876726	345.9558435
λ	0.999977238	1.37318E-05	72822.19318

Table 7. Correlation coefficient (r), Probable error (PE) and $|\frac{r}{PE}|$ values of Sh with respect to the parameters ϕ,N,S_0,λ,ω,t and K_r

parameter	r	PE	$\lvert\frac{r}{PE}\rvert$
ϕ	0.999988727	6.80059E-06	147044.3608
N	0.995223125	0.002874963	346.1690028
S0	-1	0	Inf
λ	-0.999998944	6.36994E-07	1569871.63
ω	-0.999897527	6.18179E-05	16174.89232
t	-0.983424825	0.009916783	99.16772636
K_r	-0.999970646	1.77086E-05	56468.14162

Table 8. Linear regression model for Cf, Number of observations :35, Error degrees of freedom:27, Root mean square error :0.00461, R-squared:0.989, Adjusted R-Squared 0.986, F-statistic vs. constant model:332, p-value =1.7e-24

Variables	Estimate	SE	tStat	p Value
Intercept	0.652031	0.027974	23.31551	2.02E-19
ϕ	0.654027	0.171889	3.804932	0.00074
H	-0.043	0.008129	-5.28944	1.40E-05
G_m	-0.017	0.002032	-8.36414	5.65E-09
S	-0.0108	0.003438	-3.14246	0.004041
N	0.043069	0.007597	5.669406	5.08E-06
G_r	-0.03946	0.002032	-1 .4154	2.16E-17
λ	-0.38702	0.010161	-38.0881	5.25E-25

Table 9. Linear regression model for Nu, Number of observations :20, Error degrees of freedom:15, mean square error :0.0713, R-squared: 0.995, Adjusted R- Squared 0.994, F-statistic vs. constant model:773, p-value =3.59e-17

Variables	Estimate	SE	tStat	p Value
Intercept	3.350136	0.217599	15.39591	1.34E-10
ϕ	-28.7968	3.787674	-7.60277	1.60E-06
S	0.42104	0.065763	6.402399	1.19E-05
N	-1.98807	0.168527	-11.7967	5.46E-09
λ	6.334471	0.212077	29.86876	8.87E-15

Table 10. Linear regression model for Sh, Number of observations :35, Error degrees of freedom:27, Root mean square error :0.00753, R-squared:0.998, Adjusted R-Squared 0.998, F-statistic vs. constant model:2.31e+03, p-value =8.37e-36

Variables	Estimate	SE	tStat	p value
Intercept	1.812674817	0.02908886	62.31508568	1.02898E-30
ϕ	5.495754491	0.292700432	18.77603823	5.01837E-17
N	0.034541513	0.012949556	2.667389769	0.012762683
S_0	-1.818151624	0.017165431	-105.9193681	6.57213E-37
λ	-0.594991434	0.017165431	-34.66218983	6.36399E-24
ω	-0.001988324	0.000827683	-2.402277412	0.023439152
t	-0.022729364	0.00891019	-2.550940334	0.01672498
K_r	-0.111039183	0.013732345	-8.08595936	1.09457E-08

Table 11. Comparison of Amplitude value of the coefficient, $\frac{\varepsilon}{2}e^{it}$, in the expansion of $\left(\frac{\partial \theta'}{\partial z}\right)_{z=0}$ with $\lambda = 0, N = 0, S = 0, \phi = 0$.

$\boldsymbol{\omega}$	**Sharma et al.** [41] $\left|\left(\frac{\partial \theta_1}{\partial y}\right)_{y=0}\right|$		**Present paper** $\left|\left(\frac{\partial \theta'_1}{\partial z}\right)_{z=0}\right|$	
	$\boldsymbol{P_r = 0.71}$	$\boldsymbol{P_r = 7}$	$\boldsymbol{P_r = 0.71}$	$\boldsymbol{P_r = 7}$
2	1.144	3.762	1.1438	3.7623
4	1.474	5.293	1.4745	5.2937
6	1.857	6.479	1.8575	6.4794
8	2.228	7.483	2.2289	7.4832
10	2.568	8.366	2.5668	8.3667

Table 12. Comparison of (τ_{0r}) and (β_0) of the steady flow in the absence of Ω with $G_m = 0, N = 0, K_r = 0, K_1 \to \infty, S_0 = 0, S = 0, \phi = 0, \alpha = \pi/2$.

G_r	M	H	λ	P_r	Pal and Talukdar [28]		Present paper	
					τ_{0r}	β_0	τ_{0r}	β_0
5	2	1	0.5	0.71	1.829935	0.265883	1.829935	0.265883
10	2	1	0.5	0.71	2.167691	0.206240	2.167692	0.206240
5	4	1	0.5	0.71	3.344788	0.370293	3.344789	0.370293
5	2	3	0.5	0.71	1.364854	0.255192	1.364854	0.255192
5	2	1	1	0.71	2.613122	0.142007	2.613122	0.142006
5	2	1	0.5	7	1.907705	0.246677	1.907705	0.246677

Highlights

- Theoretically and statistically examined the role of hall current, heat source and soret effects on MHD convective ferro-nanofluid (Fe3O4-water) flow through an inclined channel with porous medium.
- Velocity, thermal and concentration boundary layer in nanofluids are considered to be oscillatory.
- Heat due to radiation is induced by the huge disparity in temperature between the plates.
- Hall current is generated by the uniform application of a strong magnetic field perpendicular to the flow of fluid.
- The outcomes are displayed in the form of tables and figures using MATLAB software.
- The wall heat, mass transfer rates and surface drag are investigated through statistical tools like regression and probable error.
- Results explain that heat source and hall current has a negative impact on skin friction
- Heat source has a positive impact on Nusselt number.
- Soret number has a negative impact on Sherwood number.